PNAS RESEARCH ARTICLE | PLANT BIOLOGY OPEN ACCESS

# Gradual domestication of root traits in the earliest maize from Tehuacán

Ivan Lopez-Valdivia[a,b], Alden C. Perkins[c], Hannah M. Schneider[c], Miguel Vallebueno-Estrada[a,b], James D. Burridge[c], Eduardo González-Orozco[a], Aurora Montufar[d], Rafael Montiel[b], Jonathan P. Lynch[c,1], and Jean-Philippe Vielle-Calzada[a,1]

Edited by Matthew Hufford, Iowa State University, Ames, IA; received June 16, 2021; accepted February 14, 2022 by Editorial Board Member Dolores R. Piperno

**Efforts to understand the phenotypic transition that gave rise to maize from teosinte have mainly focused on the analysis of aerial organs, with little insights into possible domestication traits affecting the root system. Archeological excavations in San Marcos cave (Tehuacán, Mexico) yielded two well-preserved 5,300 to 4,970 calibrated y B.P. specimens (SM3 and SM11) corresponding to root stalks composed of at least five nodes with multiple nodal roots and, in case, a complete embryonic root system. To characterize in detail their architecture and anatomy, we used laser ablation tomography to reconstruct a three-dimensional segment of their nodal roots and a scutellar node, revealing exquisite preservation of the inner tissue and cell organization and providing reliable morphometric parameters for cellular characteristics of the stele and cortex. Whereas SM3 showed multiple cortical sclerenchyma typical of extant maize, the scutellar node of the SM11 embryonic root system completely lacked seminal roots, an attribute found in extant teosinte and in two specific maize mutants: *root with undetectable meristem1* (*rum1*) and *rootless concerning crown and seminal roots* (*rtcs*). Ancient DNA sequences of SM10—a third San Marcos specimen of equivalent age to SM3 and SM11—revealed the presence of mutations in the transcribed sequence of both genes, offering the possibility for some of these mutations to be involved in the lack of seminal roots of the ancient specimens. Our results indicate that the root system of the earliest maize from Tehuacán resembled teosinte in traits important for maize drought adaptation.**

maize | teosinte | domestication | root anatomy | laser ablation

## Significance

Despite their importance in supplying nutrients, root traits related to maize domestication are scarce. We used laser ablation tomography to characterize the root architecture and anatomy of 5,300-y-old maize specimens recovered from San Marcos (Tehuacán, Mexico), revealing exquisite preservation of their cellular organization. Outer cortical cells contained thick and lignified walls typical of extant maize adapted to hard soils. By contrast, the absence of seminal roots is only found in the maize ancestor, teosinte. Two genes important for seminal root development had mutations that could relate to their absence. Our results indicate that some traits related to drought adaptation were not fully present in the earliest maize from Tehuacán, providing clues to conditions prevailing during early maize cultivation.

Genetic evidence indicates that maize (*Zea mays* ssp. *mays*) populations arose from Balsas teosinte (*Zea mays* ssp. *parviglumis*, also named teosinte *parviglumis*) close to 9,000 y ago (1). This evolutionary transition caused important phenotypic changes in the aerial portion of the plant, including the partial suppression of lateral branching, a decrease in the number of male and female inflorescences per individual, the exposure of the kernel by absence of a cupulate fruitcase, and the transformation of a distichous female inflorescence that disarticulates naturally into a polystichous (3- to 12-ranked) cob with attached grains that require human intervention for dispersal (1–3). A close association has been established between some of these traits and the genes that underlie their developmental control (4, 5), or genomic regions that have lost genetic diversity as a consequence of progressive domestication (6–8). In some cases, paleogenomic analysis of millenary specimens dating to the earliest stages of Mesoamerican cultivation has allowed the establishment of reference time frame for the progression of their genetic diversity and stages of domestication (9–11).

By contrast, and despite their importance for supplying water and nutrients during all stages of growth and development, the influence of domestication on the evolution of root architecture and anatomy has received little attention. A phenotypic analysis and comparison of maize landraces and teosintes concluded that their range of root architectural and anatomical traits was similar, however, a few specific traits permitted some distinction between both subspecies (12). In general, teosintes showed less variation for architectural traits such as root system dry weight, longest nodal root length, nodal system diameter, number of root tips, and number of seminal roots. They also showed smaller mean stele and xylem areas, shorter nodal roots, less frequent lateral root branching, and significantly fewer seminal roots than landraces (12), suggesting they could be important traits affected during domestication. Comparisons of physiological responses to limited nitrogen availability indicates that teosinte *parviglumis* shows an increase of the shoot:root biomass ratio as compared to maize, as well as an increase in the length of nodal and lateral roots, but also reduced nodal root number (13). A functional decrease in major domestication genes such as *Teosinte Branched1* (Tb1) results in an increase of both lateral and nodal roots, although it remains unclear if the effect is direct or indirect (14).

Author contributions: I.L.-V., J.P.L., and J.-P.V.-C. designed research; I.L.-V., A.C.P., M.V.-E., and J.D.B. performed research; A.M. contributed new reagents/analytic tools; I.L.-V., H.M.S., E.G.-O., R.M., J.P.L., and J.-P.V.-C. analyzed data; and I.L.-V., J.P.L., and J.-P.V.-C. wrote the paper.

The authors declare no competing interest.

This article is a PNAS Direct Submission. M.H. is a guest editor invited by the Editorial Board.

Copyright © 2022 the Author(s). Published by PNAS. This open access article is distributed under Creative Commons Attribution-NonCommercial-NoDerivatives License 4.0 (CC BY-NC-ND).

[1]To whom correspondence may be addressed. Email: jpl4@psu.edu or vielle@cinvestav.mx.

This article contains supporting information online at http://www.pnas.org/lookup/suppl/doi:10.1073/pnas.2110245119/-/DCSupplemental.

Published April 18, 2022.

Root architecture is crucial for productivity by determining the temporal and spatial distribution of soil exploration and hence resource capture. Maize root architecture is comprised of embryonic and postembryonic components (15). After seed germination, the emergence of the radicle and the coleoptile is followed by the elongation of the mesocotyl. While the primary root develops from the radicle, the scutellar node gives rise to seminal roots located in a protuberance formed by the remnants of the pericarp and endosperm, located between the mesocotyl and the primary root. Seminal and primary roots are considered components of the embryonic root system. The first node forms the first nodal roots between the mesocotyl and the coleoptile. Subsequent elongation of the main vertical axis of the mesocotyl results in additional subterranean and root nodes (*SI Appendix*, Fig. S1). Aerial nodes will give rise to whorls of brace roots.

The anatomy of a root transversal section is characterized by the presence of two concentric cellular cylinders: the stele and the cortex. In maize, the central region of the differentiated stele contains xylem vessels responsible for axial transport of water and nutrients. At the periphery of each late metaxylem bundle are the smaller early metaxylem bundles. Phloem vessels, necessary for photosynthate transport, are composed of smaller cells located between late metaxylem bundles. The intersection of the cortex and the stele is composed of two concentric cell files: the pericycle and the endodermis. The cortex is composed of the root epidermis and 6 to 19 files of outer, mid, and inner cortical cells (16, 17). Cortical aerenchyma can be formed via programmed cell death. In some cases, the outer cortex exhibits multiseriate cortical sclerenchyma (MCS) with thick lignified walls, a phenotype recently reported to improve root penetration ability as an adaptation to growth in hard soils (18). Interestingly, the MCS phenotype is present in some modern maize inbreds but not in accessions of teosinte *parviglumis* and *Z. mays* ssp. *mexicana* [teosinte *mexicana;* (18)], suggesting it might represent an adaptation acquired during domestication.

Two maize genes have been shown to be important for development of seminal roots during the establishment of the embryonic root system. Mutations in *ROOT WITH UNDETECTABLE MERISTEM1* (*RUM1*) result in the absence of seminal and postembryonic lateral roots on the primary root (19–21). *RUM1* encodes a monocot specific AUX/IAA protein that can be induced by auxin. Similarly, mutants defective in *ROOTLESS CONCERNING CROWN AND SEMINAL ROOTS* (*RTCS*) completely lack seminal roots and the postembryonic shoot-borne root system (21). *RTCS* encodes a Lateral Organ Boundaries (LOB) domain protein preferentially expressed in roots. Two major quantitative loci contributing to 66% of seminal root number variation comapped with *RUM1* and *RTCS,* suggesting both genes play key regulatory functions in the development of the embryonic root system (22).

Pioneering excavations conducted in rock shelters of the Tehuacán Valley uncovered maize paleobotanical specimens dating back to the earliest stages of agriculture in Mesoamerica (23, 24), including hundreds of cob specimens, but only a few root crowns. Subsequent explorations of San Marcos cave yielded new nonmanipulated specimens dating to a similar age of 5,300 to 4,970 calibrated y B.P., including SM3, a well-preserved root crown that represents the earliest maize root specimen found to date (10). A paleogenomic analysis of SM3 and other specimens of equivalent age showed that the earliest maize from San Marcos genetically diverged from fully domesticated landraces and contained allelic variants absent from extant maize populations (10). Some domestication loci (*teosinte branched1*, *brittle endosperm2*) showed reduced nucleotide variability as compared to teosinte *parviglumis*, but others (*teosinte glume architecture1*, *sugary1*) showed conserved levels of nucleotide variability that are absent from extant maize. These temporally similar samples also showed unexpected levels of homozygosity and inbreeding, opening the possibility for Tehuacán maize cultivation evolving from reduced founder populations (10).

To characterize in detail the architecture and anatomy of the earliest maize roots found to date, we conducted laser ablation tomography (LAT) of two paleobotanic specimens (SM3 and SM11) from San Marcos cave, dating at a similar age of 5,280 to 4,956 y B.P. We generated a three-dimensional (3D) reconstruction of a second node root segment for both specimens, confirming the exquisite preservation of their inner cellular organization, and comparing multiple anatomical parameters to extant maize and teosinte accessions. SM3 exhibited MCS proposed to be exclusive to domesticated maize. By contrast, the 3D reconstruction of the scutellar node of SM11 demonstrated the absence of seminal roots, a trait only reported in extant teosintes and two specific maize mutants. Partial sequencing of *RUM1* and *RTCS* alleles present in the genome of SM10—a San Marcos specimen of equivalent age to SM3 and SM11—revealed mutations that could relate to the absence of seminal roots. Our overall results indicate that some of the most important root traits that distinguish extant maize landraces from teosinte were not fully present in the earliest maize from San Marcos.

## Results and Discussion

**Age and Root Architecture of SM3 and SM11.** Although morphometric analysis of paleobotanical specimens found in archaeological expeditions conducted in the 1960s provided important information to understand the temporal transitions that shaped domestication, high resolution capture of anatomical and architectural parameters has not been explored in ancient maize remains. We concentrated on two well-preserved specimens that were dated by accelerator mass spectrometry (AMS). SM3 is the most ancient specimen, dating to 4,220 to 4,180 $^{14}$C y B.P. (5,280 to 4,970 2$\sigma$ calibrated y B.P. at 95% confidence) (10). SM11 dated to 4,470 to 4,410 y B.P. (5280-4,880 2$\sigma$ calibrated y B.P. at 95% confidence; *SI Appendix*, Fig. S2). SM3 and SM11 are presented in Figs. 1 and 2, respectively. SM3 is a root crown containing at least five nodes with multiple nodal roots but lacking a primary root system and scutellar node (Fig. 1*A*). SM11 is a larger specimen with at least six nodes and a complete embryonic root system, notably including the scutellar node and primary root (Fig. 2*A*) (23, 24). The presence of at least five nodes in both specimens suggests that the corresponding plant individuals had reached at least the V7-V8 stage (25). Lateral roots were not preserved in either specimen. A general architectural comparison suggested that SM11 had been more drastically affected by burial compression than SM3.

We measured root architecture and anatomy parameters in SM3 and SM11, comparing their value to those previously reported for 195 accessions of maize landraces from the Americas and Caribbean islands, 36 accessions of teosinte *parviglumis*, 16 accessions of teosinte *mexicana*, and a small group of 9 additional accessions that included *Z. mays* ssp. *huehuetenangensis*, *Zea luxurians*, *Zea nicaragüensis*, and *Zea perennis* (12). The results of these comparisons are summarized and illustrated in Table 1 and Fig. 3, and *SI Appendix*, Tables S1 and S2. With

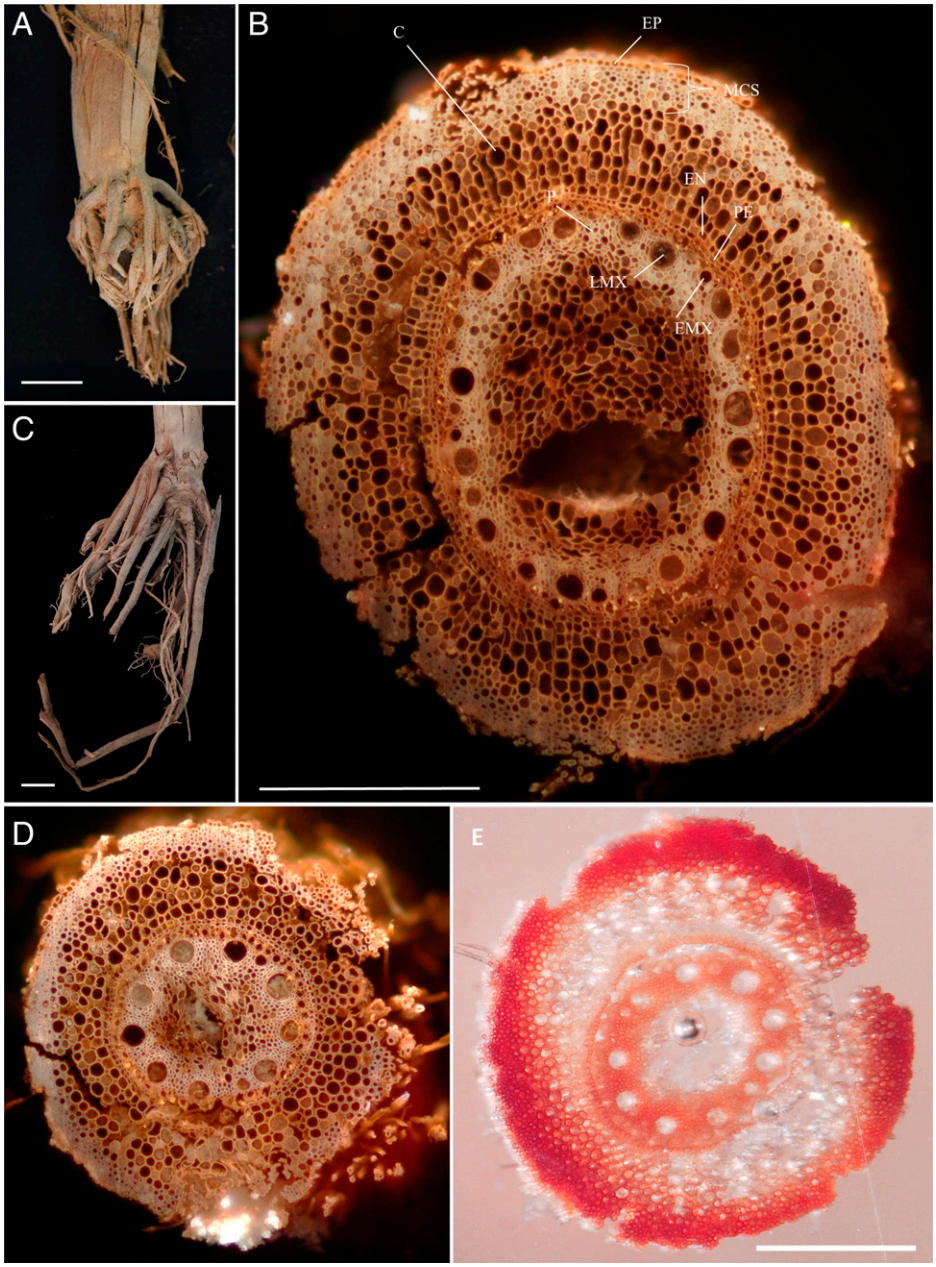


**Fig. 1.** Ancient maize root specimens from San Marcos cave. (*A*) Maize root stalk corresponding to specimen SM3 and dating 5,280 to 4,970 y B.P. (*B*) Transversal section (10 μm thick) of a nodal root belonging to specimen SM3. (*C*) Maize root stalk corresponding to specimen SM11 and dating 5,280 to 4,880 y B.P. (*D*) Transversal section of a second node root from SM3 used for lignin content determination. (*E*) Red staining of the outer cortical cells by phloroglucinol-HCl, indicating presence of lignin, a distinctive component of the MCS phenotype. Abbreviations: EP, epidermis; C, cortex; EN, endodermis; PE, pericycle; P, phloem; LMX, late metaxylem; EMX, early metaxylem. (Scale bars: *A*, 1 cm; *B*, 500 μm; *C* and *D*, 500 μm.)

the exception of the individual ancient specimens, as reported in ref. 12, all parameters were measured in three individuals per accession selected at the V6 to V7 stage, which precedes the V7 to V8 stage that had been reached by SM3 and SM11. In the case of extant landraces and teosintes, measurements were taken from 30- to 50-μm-thick cross-section segments collected 5 to 9 cm from the base of a second whorl nodal root in three different individuals per accession (12). In the case of SM3 and SM11, measurements were taken from three random 10-μm-thick cross-section LAT images of a 1-cm segment collected 5 to 9 cm from the base of a second whorl nodal root. Although the diameter of maize nodal roots can significantly vary between samples corresponding to different nodes, their characteristics tend to remain constant within the same node (12). Maize nodal roots do not undergo secondary growth, i.e., their diameter remains constant during development, from emergence to full maturity, allowing a valid comparison between previously reported parameters for extant *Zea* accessions and parameters measured at equivalent root segments and nodes from ancient specimens.

Although stem diameter (11 mm for SM3 and 14.3 mm for SM11; as compared to 15.5 ± 3.97 mm for teosinte *parviglumis*, 18.8 ± 3.1 mm for teosinte *mexicana,* and 22.8 ± 4.2 mm for mean value all maize landrace accessions) and nodal root system diameter (23.5 mm for SM3 and 32.3 mm for SM11; as compared to 43.8 ± 11.8 mm for teosinte *parviglumis*, 18.8 ± 3.1 mm for teosinte *mexicana,* and 60.9 ± 14.5 mm for maize landrace accessions) were likely affected by compression in both ancient specimens, we obtained a reliable assessment of the total number of nodal roots included in the first four nodes, making

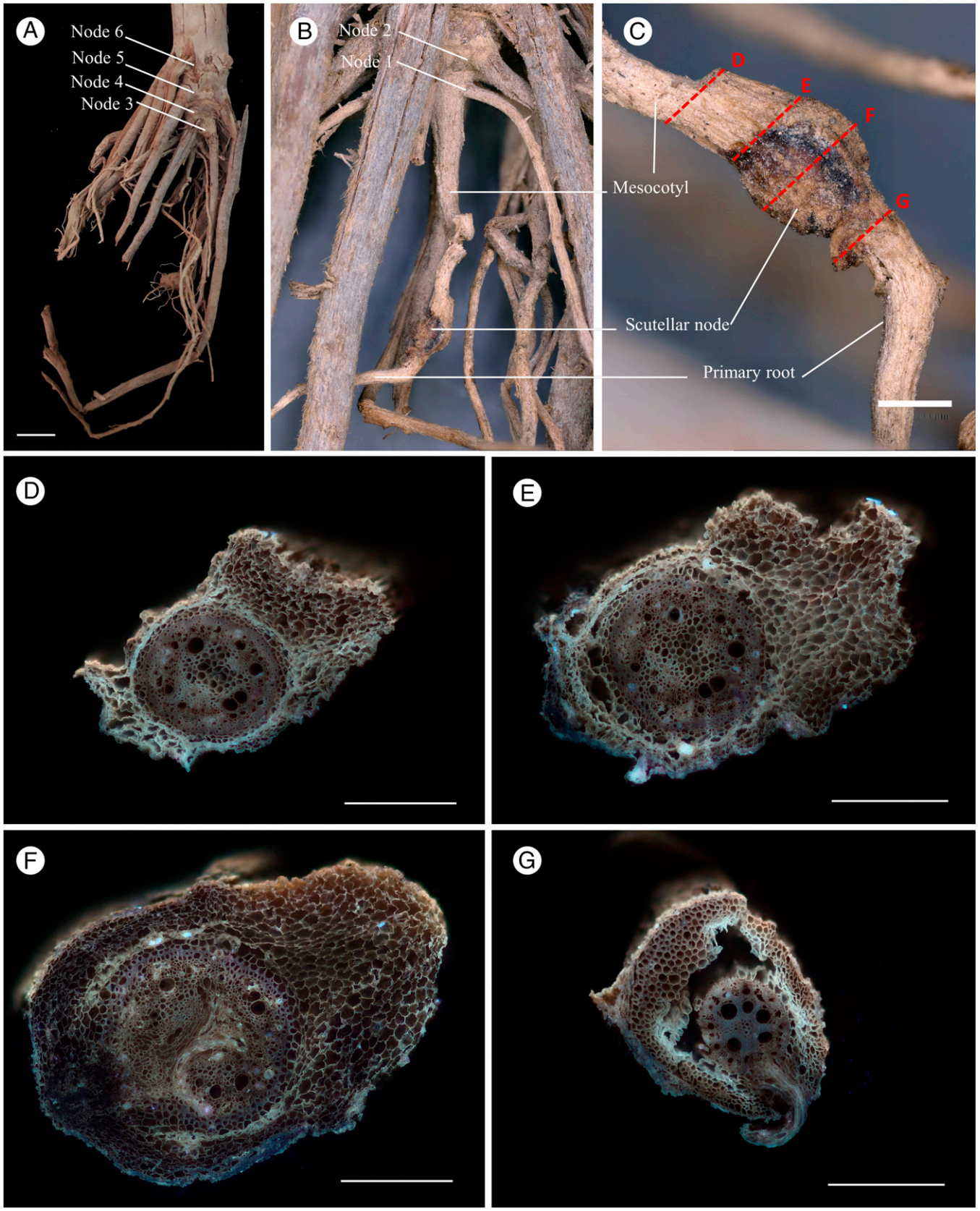


**Fig. 2.** LAT of the SM11 scutellar node and primary root. (*A*) Root architecture of SM11 depicting the presence of consecutive nodes. (*B*) Embryonic root system of SM11. (*C*) Scutellar node of SM11 showing the plane of transversal sections depicted in micrographs *D*–*G*. (*D*) Transversal section of the SM11 scutellar node top region. (*E*) Transversal section of the mid portion of the SM11 scutellar node. (*F*) Transversal section of the bottom portion of the SM11 scutellar node. (*G*) Transversal section of the primary root adjacent to the bottom part of the SM11 scutellar node. (Scale bars: 500 μm.)

**Table 1. Root architectural and anatomical trait values in extant teosintes, extant maize landraces, and 5,300 to 4,970 y B.P. maize from San Marcos cave**

| Description | Landraces ($n$ = 195), mean ± SD | SM11 | SM3 | *Teosinte parviglumis* ($n$ = 36), mean ± SD | *Teosinte mexicana* ($n$ = 16), mean ± SD | Other teosintes* ($n$ = 9), mean ± SD |
|---|---|---|---|---|---|---|
| Architectural traits | | | | | | |
| No. of nodal roots | 20.60 ± 4.2 | 21 | 25 | 23.2 ± 6.54 | 25.9 ± 6.10 | 23.4 ± 9.58 |
| No. of seminal roots | 3.90 ± 1.3 | 0 | ND | 0.47 ± 0.48 | 0.49 ± 0.45 | 0.44 ± 0.69 |
| Stem diameter, mm | 22.80 ± 4.5 | 14.3 | 11 | 15.5 ± 3.97 | 18.8 ± 3.1 | 12.4 ± 4.65 |
| Nodal root system diameter, mm | 60.90 ± 14.5 | 32.3 | 23.5 | 43.8 ± 11.8 | 49.4 ± 11.5 | 43 ± 23.2 |
| Angle | | 45.67 | 60.08 | | | |
| Anatomical traits | | | | | | |
| Cross-section area, $mm^2$ | 0.966 ± 0.258 | ND | 0.95 ± 0.0051 | 0.997 ± 0.27 | 0.933 ± 0.27 | 0.900 ± 0.352 |
| Total stele area, $mm^2$ | 0.258 ± 0.079 | 0.19 ± 0.015 | 0.22 ± 0.0018 | 0.252 ± 0.076 | 0.235 ± 0.062 | 0.195 ± 0.084 |
| Xylem vessel area, $mm^2$ | 0.053 ± 0.019 | 0.041 ± 0.0008 | 0.03 ± 0.0004 | 0.040 ± 0.009 | 0.041 ± 0.008 | 0.028 ± 0.011 |
| Aerenchyma area, $mm^2$ | 0.051 ± 0.047 | ND | 0 | 0.052 ± 0.044 | 0.054 ± 0.045 | 0.076 ± 0.111 |
| Percent of cortex as aerenchyma, % | 6.49 ± 5.25 | ND | 0 | 6.46 ± 5.02 | 6.28 ± 4.05 | 7.55 ± 8.44 |
| Total cortical area, $mm^2$ | 0.708 ± 0.187 | ND | 0.74 ± 0.0068 | 0.745 ± 0.199 | 0.698 ± 0.211 | 0.705 ± 0.27 |
| Cortical cell traits | | | | | | |
| No. of cortical cells | 596 ± 141 | ND | 1,272 ± 151 | 602 ± 144 | 582 ± 101 | 595 ± 157 |
| No. of cortical cells files | 9.96 ± 1.09 | ND | 13.67 ± 0.47 | 10.1 ± 1.0 | 9.89 ± 1.25 | 10.1 ± 1.25 |
| Inner cortical cell size, $\mu m^2$ | ND | ND | 530.32 ± 72.78 | ND | ND | ND |
| Middle cortical cell size, $\mu m^2$ | ND | ND | 1,045.45 ± 91.12 | ND | ND | ND |
| Outer cortical cell size, $\mu m^2$ | ND | ND | 94.05 ± 30.12 | ND | ND | ND |

ND: not determined.
*_Z. perennis_ (5); _Z. luxurians_ (1); _Z. huehuetenangensis_ (1); Z. _nicaragüensis_ (1); F1 B73 X _Z. diploperrenis_ hybrid (1).

our values comparable to mean estimations previously reported for extant teosintes and maize landraces (12). By taking into consideration all root segments and scars, SM3 and SM11 contained 25 and 21 nodal roots in the first four nodes, respectively, a range within mean values previously reported for all teosinte (23.2 ± 6.5 for teosinte *parviglumis* and 25.9 ± 6.1 for teosinte *mexicana)* and maize landrace accessions (20.6 ± 4.2). Although both one-way ANOVA and Tukey's statistical tests suggested significant differences between teosinte and maize accessions in the total number of nodal roots (Fig. 3*A*), the SM3 and SM11 values did not permit a clear distinction of teosinte versus maize for this trait in any of the two specimens. The embryonic root system was not present in SM3, whereas the scutellar node of SM11 did not show any remnants of seminal roots. Previously reported results showed significant differences in the average number of seminal roots between teosinte (0.47 ± 0.48 for teosinte *parviglumis*, 0.49 ± 0.45 for teosinte *mexicana,* 0.44 ± 0.69 for the small group of distinct teosinte subspecies and species) and maize accessions (3.9 ± 1.3) (12), suggesting that this architectural trait in SM11 is reminiscent of teosinte and not extant maize landraces (Fig. 3*A*).

**Root Anatomy of SM3 and SM11.** LAT allows detailed quantitative and qualitative morphometric analysis of root anatomy and 3D reconstruction of selected root portions, providing new opportunities to assess and compare traits related to domestication. LAT consists of a pulsed ultraviolet (UV) laser that oscillates in an ablation plane as a sample is moved into with a mechanical stage, permitting a camera focused on the ablation plane to capture images resulting from UV fluorescence emission of the ablated tissue (26). To determine the degree of inner preservation of both specimens, we conducted LAT of a 7- mm segment of a second node root of both SM3 and SM11, capturing a cross-sectional image every 10 μm (for a total of 700 images), and allowing comparison with current standard measurements conducted in extant teosinte and maize accessions. In both samples the inner cell contour and organization remained intact when soil compression did not affect root structure (Fig. 1*B* and *SI Appendix*, Fig. S3). In SM3, the central cylinder, stele, and cortex were clearly distinguishable, showing detailed preservation of xylem, phloem, pericycle, and endodermal cells, as well as several files of cortical cells and a well-defined epidermis (Fig. 1*B*). The total transversal cross-sectional area of the analyzed SM3 nodal root segment (RXSA) was 0.95 $mm^2$ (Table 1), a value that is similar to the mean RXSA previously reported for teosinte and maize (0.997 ± 0.27 $mm^2$ for teosinte *parviglumis*, 0.933 ± 0.27 $mm^2$ for teosinte *mexicana*, and 0.966 ± 0.280 $mm^2$ for maize landraces). By contrast, the cortex of SM11 was partially collapsed (*SI Appendix*, Fig. S3), but the stele remained intact, allowing a reliable measurement of xylem and stele area, as described below.

***Cortical cell number, files, and size of SM3.*** Cortical phenotypes were only observed in SM3, since SM11 exhibited extensive collapse of its cortex. The total cortical area (TCA) of a transversal section of a SM3 second node root was 0.74 ± 0.006 $mm^2$, a value slightly higher than the mean TCA previously reported for teosinte and maize (0.727 ± 0.211 $mm^2$ for all teosintes included in the analysis; 0.745 ± 0.199 for teosinte *parviglumis*; 0.698 ± 0.211 for teosinte *mexicana*; and 0.708 ± 0.187 for maize landraces; Table 1). Strikingly, it contained an average of 1,272 ± 151 cortical cells (#CC), a number significantly greater than mean values for teosinte and maize reported

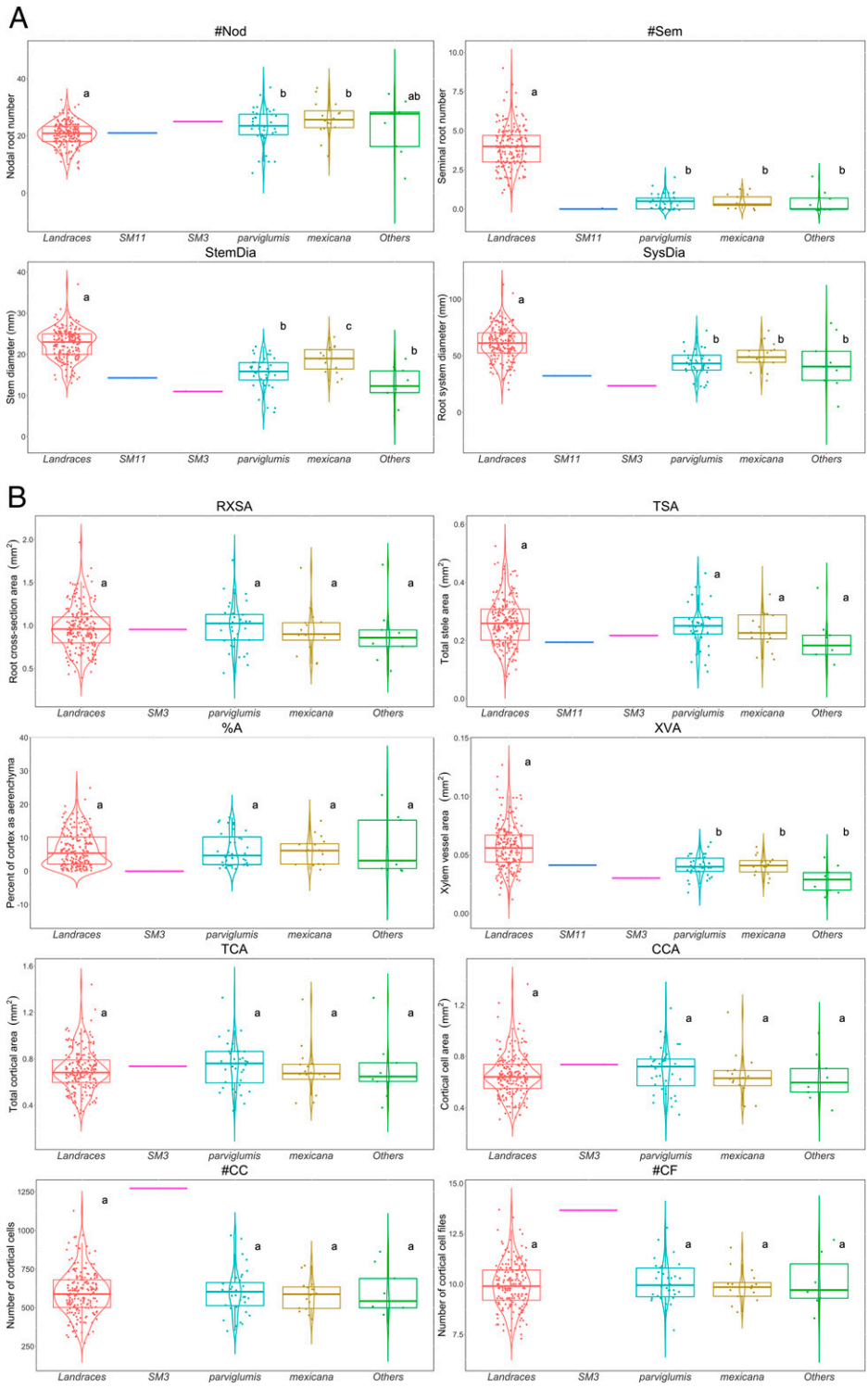


**Fig. 3.** Comparison of root architectural and anatomical parameters in extant teosintes, extant maize landraces, and 5,300 to 4,970 y B.P. maize from San Marcos cave. (*A*) Architectural parameters. (*B*) Anatomical parameters. Letters indicate significant (a-b) or nonsignificant (a-a) differences between extant teosinte and maize distributions following both one-way ANOVA and Tukey's honest significant test. SM3 values are represented in green and SM11 values in brown.

to date (595.7 ± 134.5 for all teosintes included in the analysis; 602 ± 144 for teosinte *parviglumis*; 582 ± 101 for teosinte *mexicana;* 596 ± 141 for maize landraces). The mean number of cortical cell files (#CF) of SM3 was also significantly greater than those previously reported for extant accessions: 13.67 ± 0.47, as compared to 10.1± for teosinte *parviglumis*, 9.89 ± 1.25 for teosinte *mexicana,* and 9.96 ± 1.09 for maize landraces. Cortical cells of SM3 were heterogeneous in size. The average inner cortical cell size (CCS) and middle CCS cortical cell size was 530.32 ± 72.78 and 1045.45± 91.12 μm$^2$, respectively, whereas the average outer CCS was 94.04 ± 30.12 μm$^2$. In general, CCS in maize is substantially variable across the root cortex, with cells presenting the largest cross-sectional area located in the center and reducing size toward the periphery. Previous studies reported 6 to 19 cortical cell files in maize in second node roots (16), and maximum values of cross-

sectional area of cortical cells comprised between 514.6 and 533.9 $\mu m^2$ (27), a range close to 50% smaller than values obtained for mean middle CCS size in SM3. A CCS within the range of those shown by SM3 has not previously been reported in extant maize.

***Stele and xylem area of SM3 and SM11.*** Whereas extant teosintes and maize landraces exhibit equivalent values of RXSA (Table 1) on the basis of previously reported results (12), total stele area (TSA) tend to be greater in extant landraces as compared to teosinte accessions (0.258 ± 0.079 $mm^2$ for landraces vs. 0.252 ± 0.076 $mm^2$ for teosinte *parviglumis* and 0.235 ± 0.062 $mm^2$ for teosinte *mexicana*). The same is true for mean xylem vessel area (XVA; 0.053 ± 0.019 $mm^2$ for landraces vs. 0.04 ± 0.009 $mm^2$ for teosinte *parviglumis* and 0.041 ± 0.008 $mm^2$ for teosinte *mexicana*) We measured both parameters in SM3 and SM11. TSA values were 0.22 ± 0.0018 $mm^2$ and 0.19 ± 0.015 $mm^2$, respectively, whereas XVA values were 0.03 ± 0.0004 $mm^2$ and 0.041 ± 0.0008 $mm^2$. Although one-way ANOVA and Tukey's test suggested significant differences in XVA between teosinte and maize populations (Table 1), the SM3 and SM11 values tend to be smaller than the average value for maize, however, the values did not allow a clear discrimination between the two groups.

***Presence of MCS in SM3.*** The exquisite preservation of the epidermis and cortex of the SM3 second node crown root segment allowed the identification of outer cortical cell files with substantial reduction in cell size as compared with the rest of the cortex, a phenotype indicative of MCS (Fig. 1*B* and *SI Appendix*, Fig. S4). These cells had an average area of 94.04 $\mu m^2$, whereas middle and inner cortical cells had an average area of 530.32 $\mu m^2$ and 1045.45 $\mu m^2$, respectively. Maize lines with MCS have a wall-to-lumen ratio ranging from 2.1 to 4.4, whereas the same ratio ranges from 0.4 to 2.2 in non-MCS maize lines (18). The average wall-to-lumen ratio of the outer SM3 sclerenchyma was 4.1 ± 0.11 $\mu m^2$, a high value within the MCS range. The presence of outer cortical cells with enlarged cell walls and small cell lumen was fully confirmed by cryoscanning electron microscopy of a second node crown root segment containing MCS cell walls with a thickness comprised between 3.5 and 4 μm (*SI Appendix*, Fig. S4). Histological staining of SM3 root segments with phloroglucinol-HCl demonstrated that thickening of cell walls in MCS is primarily due to the presence of lignin (Fig. 1 *C* and *D*). The nonrandom specific deposition of lignin in the outer cortical cells corresponds to the previously reported MCS phenotype found in extant maize but not in teosinte *parviglumis* or *mexicana* accessions (18).

**Linear Discriminant Analysis for SM3 and SM11.** To determine if root architecture and anatomy could be used as phenotypes to separate teosintes from extant maize landraces, we trained a linear discriminant analysis (LDA) model with a set of parameters that included number of nodal roots (#Nod), diameter of the root system (SysDia), diameter of the stem (StemDia), RXSA, TCA, TSA, percentage of cortex aerenchyma (%A), cortical cell area, XVA, number of cortical cells (#CC), and number of cortical cell files (#CF) (model 1), using previously reported values for 41 teosintes (*parviglumis* and *mexicana*), 172 maize landraces, and two inbred lines (12, 28, 29, 30). The resulting model was independently tested with 20 teosintes, 20 maize landraces, and SM3 as an outgroup. The results are presented in the *SI Appendix*, Table S3 and Fig. S5. In the case of teosintes and landraces, Model 1 correctly predicted the corresponding group in 90% of the cases (18 out of 20 teosintes; 18 out of 20 landraces; *SI Appendix*, Table S1). On the basis of this level of confidence, SM3 was predicted to belong to teosinte class with a probability close to 1. A second LDA model included #Nod, number of seminal roots (#Sem), SysDia, TSA, and XVA (model 2, *SI Appendix*, Table S3), and was trained with values from the same collection of germplasm as model 1. Model 2 correctly predicted the corresponding group in 95% of the cases (19 out of 20 teosintes; 19 out of 20 landraces). On the basis of this second level of confidence, SM11 was predicted to belong to teosinte class with a probability of 0.99. These results suggest that root phenotypes in both maize specimens tend to resemble teosinte rather than maize landraces.

**Three-Dimensional Reconstruction of the SM11 Scutellar Node.** In SM11, high-resolution imaging of the scutellar node surface suggested that seminal roots did not develop as part of the embryonic root system. To confirm the absence of seminal roots in SM11, we generated and analyzed a 3D reconstruction of the complete scutellar node. As shown in the *SI Appendix*, Fig. S6, transversal sections of the scutellar node in teosinte *parviglumis* and extant maize landraces show that seminal roots emerge from inner cell files, at the boundaries of central cylinder. Seminal roots emerge from primordia extending from the central core across dozens of cell files before reaching the node surface. In SM11, root primordia or root extensions were completely absent from the scutellar node (Fig. 2 *B*–*G*). The only root extension identified in the 3D reconstruction was a lateral root emerging from the primary root, outside the bottom part of the scutellar node (Fig. 2*G*). This evidence indicates that SM11 corresponds to a plant that did not develop seminal roots, a phenotypic feature that is specific to extant teosinte and not maize.

**Molecular Analysis of *RUM1* and *RTCS*.** In addition to SM3 and SM11, excavations at San Marcos cave uncovered specimen SM10, a cob previously dated to 4,240 ± 30 $^{14}C$ y B.P. (5,300 to 5,040 2$\sigma$ calibrated y B.P. at 95% confidence). Whereas SM3 and SM11 had a poor representation of reads mapping to unique genomic regions, analysis of the SM10 aDNA yielded 1.26 Gb coverage of the nonrepetitive maize genome (10). To indirectly test the possibility that *RUM1* (GRMZM2G037368) or *RTCS* (GRMZM2G092542) could be involved in the lack of seminal roots characterizing the SM11 embryonic root system, we analyzed ancient DNA sequences from SM10. We aligned SM10 reads to the *RUM1* and *RTCS* transcribed sequence in the B73 genome and 26 recently reported de novo assembled genomes (ref. 19; *SI Appendix*, Tables S4 and S5 and Figs. S7–S10). Among more than 19.7 million reads mapping to unique genomic regions, we recovered 52 corresponding to the transcribed sequence of *RUM1*, and 14 corresponding to the transcribed sequence of *RTCS*, with an average length of 88.46 (*RUM1*) and 79.78 (*RTCS*) nucleotides (nt) per read, respectively (*SI Appendix*, Table S4). These sequences resulted in a segmental coverage of 62.47% of the *RUM1* and 43.64% of the *RTCS* transcribed region. Although the average coverage depth (1.8×) was not sufficient to ensure a reliable determination of the SM10 diploid genotype, several sequences included variants with respect to the B73 reference sequence. We identified 42 single nucleotide variants (SNVs) included in the ancient sequence of *RUM1* (*SI Appendix*, Fig. S7), with six located within exons and seven within untranslated regions (UTRs). We also identified a deletion of eleven nucleotides located 33 nt upstream of the 3′UTR end. This deletion was

also found in the *RUM1* sequence of four additional genomes (Zm-Oh43, Zm-M37W, Zm-Ky21, and Zm-Ki3; *SI Appendix*, Fig. S9), suggesting its presence prevailed in some extant lineages. In the case of *RTCS*, we identified 13 SNVs; 3 are located in exons and 10 in the UTRs (*SI Appendix*, Fig. S8). Interestingly, a SNV located in the second exon generates a STOP codon that was not found in any of the 25 extant genomes analyzed (*SI Appendix*, Fig. S10), suggesting possible detrimental effects subsequently purified by negative selection. None of the teosinte and maize diversity datasets analyzed (HapMap3, MaizeSNP50 BeadChip, and maize GBS2.7; (27)) reports SNPs at the *RUM1* deletion or *RTCS* STOP codon site. Although our limited coverage is unable to confirm the homozygous nature of the mutations described above, their identification opens the possibility for these genes to be involved in the lack of seminal roots shown by SM11.

Although many phenotypic traits related to the architecture and anatomy of the root system are not distinguishable between teosintes and maize, large-scale phenotypic analysis of extant accessions suggests that XVA and the #Sem are significantly different between extant maize landraces and their teosinte ancestors (12). The value of these parameters is remarkably conserved among teosinte accessions, even within different taxa. The presence of MCS also distinguishes teosintes from maize (18). XVA values for both ancient specimens did not allow to establish a tendency to resemble extant teosinte or maize accessions. By contrast, the presence of MCS in the outer cortex of SM3, and the absence of seminal roots developing in the scutellar node of SM11, suggest that some of the maize root phenotypes found in extant accessions were present in 5,300 to 4,790 y B.P. maize, but others were not. Although MCS is absent from seven previously analyzed teosinte *parviglumis* and three teosinte *mexicana* accessions, a larger sampling is required to confirm its eventual condition of a maize specific root trait. Extant maize lines with MCS are better adapted to mechanical impedance by increasing root depth by 22% and producing 39% more biomass in soils compacted by vehicle traffic (18). Whereas the large size of SM3 cortical cells could represent an ancestral adaptation causing a reduction of metabolic costs (28), a combination of small XVA (31), large mCCS (32), and the presence of MCS (18), could contribute to establish an integrated phenotype adapted to drought. An equivalent integrated phenotype is associated with superior drought tolerance in extant maize (31). Taking aside mutations in *RUM1* and *RTCS*, the absence of seminal roots has been rarely reported in extant maize accessions. Seminal roots are beneficial for phosphorus capture in maize (33). A recent in silico study suggests that although seminal roots are indeed beneficial for capturing both phosphorus and nitrogen, teosinte cannot form seminal roots due to limited seed carbohydrate reserves (34). In addition to teosintes, a reduced number of seminal roots has also been reported in wild wheat and barley, suggesting a possible adaptation to water stress (35, 36), or a possible consequence of a reduced seed endosperm that restricts seminal root formation in these wild taxa (34). Earlier studies indicated that, under nonlimiting soil phosphate availability, the probability for extant maize individuals to lack seminal roots is close to null; under low soil phosphate conditions, the probability is close to 0.02 (33). Under these assumptions, the absence of seminal roots in SM11 is unlikely due to nutritional adaptation, but rather caused by seed phenotypic traits—and their genetic control—that brought the embryonic root system of the earliest Tehuacán maize to closely resemble extant teosintes. Our overall results suggest that selection affected some maize root traits late during domestication, with human selection progressing at different temporal rates in the aerial and subterranean organs. While X-ray microscopy 3D technologies promise to refine the nondestructive internal analysis of paleobotanical remains (37), our study demonstrates the value of LAT for the phenotypic analysis of paleobotanical root specimens, opening new possibilities for the identification of domestication traits selected during the transition from teosinte to maize.

## Materials and Methods

**Archaeobotanical Specimens and Dating.** SM3 and SM10 are specimens discovered during the 2012 Langebio Cinvestav–Instituto Nacional de Antropología e Historia (INAH) expedition to San Marcos cave, as previously reported (10). SM11 is a maize root stalk found during MacNeish expeditions (1961 to 1962) and curated by the INAH. Using the service provided by Beta Analytic, 10 to 20 mg of each specimen was dated with AMS.

**Estimation of Root Architecture Parameters.** Specimens were observed, analyzed, and photographed using a Keyence VHX high resolution digital microscope with a 20 and 50× magnification lens. General specimen images were captured using a Nikon D3300. A ruler in centimeters was included in each image as a scale reference. Stem diameter was measured at the most basal node of the brace roots, while the diameter of the root system was measured at the widest section of the root network. The number of nodal roots per node was counted manually. Root angle was estimated by measuring the distance from the most basal part of the stem to the maximum diameter of the root network. These two parameters were subsequently used to determine the main vertical axis of the specimen and the external point to the periphery of the root network. The root angle is the angle comprised between the main vertical axis with the axis emerging from the intersection of the main vertical axis and the widest point intersecting with the external root network. Image analysis was performed using RSAJ (38) and ObjectJ (39) plugins.

**LAT and Estimation of Root Anatomy Parameters.** To precisely adjust sampling procedures to those described in ref. 12, an ∼1-cm-long segment collected 5 to 9 cm from the base of a second node root was sectioned from SM3 and SM11 specimens. LAT was used to obtain images of transversal root sections. LAT consists of a pulsed UV laser (s-Pulse HP, 343 nm THG, Amplitude Systems) that oscillates in the focal plane of a camera ($\alpha$7R III digital camera, Sony. MP-65 mm F/2.8 Lens photo macro 1–5, Canon). The transversal root segment is perpendicularly placed in front of the laser beam that vaporizes the sample while the camera captures the cross-sectional image. For each sample, 7-mm-wide transversal segments were captured, capturing an image every 10 μm, for a total of 700 images. The 3D animations were created by stacking all 700 images with Avizo 9 lite software (VSG Inc). Root anatomy parameters were measured by selecting three random images for each sample using the RootScan 2.3v software (38, 41) and calculating the average values for each parameter presented in Table 1. The same procedure was used for estimating cortical cell area from inner, middle, and outer cortical regions with imageJ (42). To phenotype MCS, the ratio of cell wall to lumen area in the outer cortex was determined using MIPAR software (43). In specimen SM11, the scutellar node and a fraction of the primary root and the mesocotyl were also analyzed by LAT.

**Histology.** For determining the cellular localization of lignin, 400-μm-thick transversal sections of a second node SM3 root were generated using LAT, and directly stained with a 3% (wt/vol) phloroglucinol solution in ethanol for 10 min. After rinsing with deionized water, sections were mounted in conventional slides and observed under a Nikon SMZ1500 microscope using bright field illumination.

**Cryoscanning Electron Microscopy.** A second node root segment of specimen SM3 was directly mounted, embedded in liquid nitrogen, and transferred to a cryopreservation chamber to withdraw the holder under vacuum. The sample was subsequently transferred to a SEM chamber and analyzed with a Zeiss Sigma VPFESEM microscope at temperature and voltage of 195 °C and 10 kV, respectively.

**Statistical Analysis.** Mean and SD values for architectural and anatomical root parameters in extant maize landraces and teosintes were obtained from data previously reported in ref. 12 and corresponding to 195 maize landrace accessions from a wide diversity of countries in North, Central and South America, as well as the Caribbean islands, and 61 teosinte accessions that included 36 of *Zea mays* ssp. *parviglumis,* 16 of *Zea mays* ssp. *mexicana,* 1 of *Zea mays* ssp. *huehuetenangensis,* 5 of *Z. perennis,* 1 of *Z. luxurians,* 1 of *Z. nicaragüensis*, and 1 hybrid (B73 inbred line per *Z. mays* ssp. *diploperennis*). For extant landraces and teosintes, values correspond to overall measurements of a 30- to 50-μm-thick cross-section segment collected 5 to 9 cm from the base of a second whorl nodal root in three different individuals per accession. In the case of SM3 and SM11 ancient specimens, values correspond to measurements in three random 10-μm-thick cross-section images of a 1-cm segment collected 5 to 9 cm from the base of a second whorl nodal root. One-way ANOVA and Tukey's honest significant tests were conducted to compare extant teosinte to extant maize distributions using R v. 4.0.0 (43). Graphs were created with the ggplot2 package (43, 44). An LDA was conducted using MASS (44). Since available parameters for SM3 were not identical than parameters available for SM11, an independent model was developed for each specimen. In the case of SM3, the LDA model was trained with stem diameter, root system diameter, number of nodal roots, nodal root transversal area, total cortical area, total stele area, percentage of aerenchyma, cortical cell area, xylem vessel area, number of cortical cells, and number of cortical cell files. In the case of SM11, the LDA model was trained with stem diameter, number of seminal roots, number of nodal roots, root system diameter, TSA, and XVA. In both cases, parameter values to train the model were obtained from ref. 12 by including 172 maize landraces, 41 teosintes, and 2 inbred lines (12, 29, 30).

**Ancient DNA Analysis.** All SM10 genomic reads corresponding to nonrepetitive regions are reported in ref. 10. Filtered quality reads corresponding to the transcribed sequence of *RUM1* (RMZM2G037368) and *RTCS* (GRMZM2G092542) were aligned to the B73 reference genome (MaizeGDB 3.0) using Burrows-Wheeler Aligner (45). Translational alignment visualization was generated with Tablet (46). The *RUM1* eleven nucleotide deletion of specimen SM10 initiates in coordinate Chr3:209176295; the *RTCS* SNV causing a STOP codon is located in coordinate Chr1:10825088. Both were searched as SNPs in datasets HapMap3, MaizeSNP50 BeadChip, and maize GBS2.7 (27), but neither was included in those analyses.

**Data Availability.** All study data are included in the article and/or supporting information. Previously published data were used for this work (*SI Appendix,* Table S1). Architecture parameter values of teosinte and landrace accessions are as reported in ref. 12.

**ACKNOWLEDGMENTS.** We thank Peter Ilhardt and Michael Williams for technical help during laser ablation tomography, and Jagdeep Singh Sidhu for support during cryoscanning electron micrscopy performed at the Penn State Cryo-Electron Microscopy Facility (University Park, PA). I.L.-V, E.G.-O., and M.V.-E. were recipients of a graduate scholarship from Consejo Nacional de Ciencia y Tecnología (CONACyT). Work in the United States was supported by the National Institute of Food and Agriculture, US Department of Agriculture (Grants 2017–67013–26192 and 2021-67013-33723), and US Department of Energy ARPA-E Award DE-AR0000821. Work in Mexico was supported by CONACyT Grant CB256826 and the Instituto Nacional de Antropología e Historia, through the Cinvestav–INAH collaboration.

Author affiliations: [a]Grupo de Desarrollo Reproductivo y Apomixis, Unidad de Genómica Avanzada, Laboratorio Nacional de Genómica para la Biodiversidad, Cinvestav, Irapuato 36821 Guanajuato, Mexico; [b]Grupo de Interacción Núcleo-Mitocondrial y Paleogenómica, Unidad de Genómica Avanzada, Laboratorio Nacional de Genómica para la Biodiversidad, Cinvestav, Irapuato 36821 Guanajuato, Mexico; [c]Department of Plant Science, Pennsylvania State University, State College, PA 16802; and [d]Subdirección de Laboratorios y Apoyo Académico, Instituto Nacional de Antropología e Historia, CP6010 Ciudad de México, Mexico

1. Y. Matsuoka *et al.*, A single domestication for maize shown by multilocus microsatellite genotyping. *Proc. Natl. Acad. Sci. U.S.A.* **99**, 6080–6084 (2002).
2. B. F. Benz, Archaeological evidence of teosinte domestication from Guilá Naquitz, Oaxaca. *Proc. Natl. Acad. Sci. U.S.A.* **98**, 2104–2106 (2001).
3. J. F. Doebley, B. S. Gaut, B. D. Smith, The molecular genetics of crop domestication. *Cell* **127**, 1309–1321 (2006).
4. H. Wang, A. J. Studer, Q. Zhao, R. Meeley, J. F. Doebley, Evidence of the origin of naked kernels during maize domestication was caused by a single amino acid substitution in tga1. *Genetics* **200**, 965–974 (2015).
5. A. J. Studer, H. Wang, J. F. Doebley, Selection during maize domestication targeted a gene network controlling plant and inflorescence architecture. *Genetics* **207**, 755–765 (2017).
6. M. B. Hufford *et al.*, Comparative population genomics of maize domestication and improvement. *Nat. Genet.* **44**, 808–811 (2012).
7. M. G. Stetter, K. Thornton, J. Ross-Ibarra, Genetic architecture and selective sweeps after polygenic adaptation to distant trait optima. *PLoS Genet.* **14**, e1007794 (2018).
8. Q. Chen *et al.*, The genetic architecture of the maize progenitor, teosinte, and how it was altered during maize domestication. *PLoS Genetics* **16**, e1008791 (2020).
9. J. Ramos-Madrigal *et al.*, Genome sequence of a 5,310 year old maize cob provides insights into the early stages of maize domestication. *Curr. Biol.* **26**, 3195–3201 (2016).
10. M. Vallebueno-Estrada *et al.*, The earliest maize from San Marcos Tehuacán is a partial domesticate with genomic evidence of inbreeding. *Proc. Natl. Acad. Sci. U.S.A.* **113**, 14151–14156 (2016).
11. L. Kistler *et al.*, Multiproxy evidence highlights a complex evolutionary legacy of maize in South America. *Science* **362**, 1309–1313 (2018).
12. A. Burton, K. M. Brown, J. P. Lynch, Phenotypic diversity of root anatomical and architectural traits in *Zea* species. *Crop Sci.* **53**, 1042–1055 (2013).
13. A. Gaudin, S. McClymont, M. Raizada, The nitrogen adaptation strategy of the wild teosinte ancestor of modern maize, *Zea mays* subsp. *parviglumis. Crop Sci.* **51**, 2780–2795 (2011).
14. A. C. Gaudin, S. A. McClymont, S. S. Soliman, M. N. Raizada, The effect of altered dosage of a mutant allele of Teosinte branched 1 (*tb1-ref*) on the root system of modern maize. *BMC Genet.* **15**, 23 (2014).
15. J. L. Bennetzen, S. C. Hake, "The maize root system: Morphology, anatomy and genetics" in *Handbook of Maize: Its Biology*, F. Hochholdinger, Ed. (Springer, 2009), pp. 145–160.
16. J. G. Chimungu, K. M. Brown, J. P. Lynch, Reduced root cortical cell file number improves drought tolerance in maize. *Plant Physiol.* **166**, 1943–1955 (2014).
17. R. Crang, S. Lyons-Sobaski, R. Wise, "Roots" in *Plant Anatomy* (Springer, ed. 2, 2019), pp. 332–342.
18. H. M. Schneider *et al.*, Multiseriate cortical sclerenchyma enhance root penetration in compacted soils. *Proc. Natl. Acad. Sci. U.S.A.* **118**, e2012087118 (2021).
19. M. B. Hufford *et al.*, De novo assembly, annotation, and comparative analysis of 26 diverse maize genomes. *Science* **373**, 655–662 (2021).
20. I. von Behrens *et al.*, Rootless with undetectable meristem 1 encodes a monocot-specific AUX/IAA protein that controls embryonic seminal and post-embryonic lateral root initiation in maize. *Plant J.* **66**, 341–353 (2011).
21. G. Taramino *et al.*, The maize (*Zea mays* L.) RTCS gene encodes a LOB domain protein that is a key regulator of embryonic seminal and post-embryonic shoot-borne root initiation. *Plant J.* **50**, 649–659 (2007).
22. S. Salvi *et al.*, Two major quantitative trait loci controlling the number of seminal roots in maize co-map with the root developmental genes rtcs and rum1. *J. Exp. Bot.* **67**, 1149–1159 (2016).
23. R. S. MacNeish, "A summary of the subsistence" in *The Prehistory of the Tehuacan Valley. Volume 1: Environment and Subsistence*, D. Byers, Ed. (University of Texas Press, Austin, TX, 1967), pp. 290–309.
24. P. C. Mangelsdorf, *Corn Its Origin, Evolution and Improvement.* (Belknapp Press, 1974).
25. J. Ransom, G. Endres, *Corn Growth and Management: Quick Guide* (North Dakota State University Extension Service, Fargo, ND, 2014).
26. C. F. Strock *et al.*, Laser ablation tomography for visualization of root colonization by edaphic organisms. *J. Exp. Bot.* **70**, 5327–5342 (2019).
27. J. C. Glaubitz *et al.*, TASSEL-GBS: A high capacity genotyping by sequencing analysis pipeline. *PLoS One* **9**, e90346 (2014).
28. J. G. Chimungu, K. M. Brown, J. P. Lynch, Large root cortical cell size improves drought tolerance in maize. *Plant Physiol.* **166**, 2166–2178 (2014).
29. A. L. Burton *et al.*, QTL mapping and phenotypic variation for root architectural traits in maize (*Zea mays* L.). *Theor. Appl. Genet.* **127**, 2293–2311 (2014).
30. A. L. Burton *et al.*, QTL mapping and phenotypic variation of root anatomical traits in maize (*Zea mays* L.). *Theor. Appl. Genet.* **128**, 93–106 (2015).
31. S. P. Klein, H. M. Schneider, A. C. Perkins, K. M. Brown, J. P. Lynch, Multiple integrated root phenotypes are associated with improved drought tolerance in maize. *Plant Physiol.* **183**, 1011–1025 (2020).
32. D. J. Vanhees, K. W. Loades, A. G. Bengough, S. J. Mooney, J. P. Lynch, Root anatomical traits contribute to deeper rooting of maize under compacted field conditions. *J. Exp. Bot.* **71**, 4243–4257 (2020).
33. J. Zhu, S. M. Mickelson, S. M. Kaeppler, J. P. Lynch, Detection of quantitative trait loci for seminal root traits in maize (*Zea mays L.)* seedlings grown under differential phosphorus levels. *Theor. Appl. Genet.* **113**, 1–10 (2006).
34. A. C. Perkins, J. P. Lynch, Increased seed carbohydrate reserves associated with domestication influence the optimal seminal root number of Zea mays. *bioRxiv* [Preprint] (2020). https://www.biorxiv.org/content/10.1101/2020.12.09.417691v1. Accessed 9 December 2020.
35. S. Grandom, S. Ceccarelli, Seminal root morphology and coleoptile length in wild (*Hordeum vulgare* ssp. spontaneum) and cultivated (*Hordeum vulgare* ssp. vulgare) barley. *Euphytica* **86**, 73–80 (1995).
36. G. Golan, E. Hendel, G. E. Méndez Espitia, N. Schwartz, Z. Peleg, Activation of seminal root primordia during wheat domestication reveals underlying mechanisms of plant resilience. *Plant Cell Environ.* **41**, 755–766 (2018).
37. K. E. Duncan, K. J. Czymmek, N. Jian, A. C. Thies, C. N. Topp, X-ray microscopy enables multiscale high-resolution 3D imaging of plant cells, tissues and organs. *Plant Physiol.* **188**, 831–845 (2022).
38. N. Vischer, S. Nastase, ObjectJ. http://simon.bio.uva.nl/objectj/index.html. Accessed 29 March 2022.
39. L. M. York, T. Galindo-Castañeda, J. R. Schussler, J. P. Lynch, Evolution of US maize (*Zea mays* L.) root architectural and anatomical phenes over the past 100 years corresponds to increased tolerance of nitrogen stress. *J. Exp. Bot.* **66**, 2347–2358 (2015).

40. B. Burton, M. Williams, J. P. Lynch, K. M. Brown, RootScan: Software for high-throughput analysis of root anatomical traits. *Plant Soil* **357**, 189–203 (2012).
41. M. D. Abramoff, P. J. Magalhaes, S. J. Ram, Image processing with ImageJ. *Biophotonics Int.***11**, 36–42 (2004).
42. J. M. Sosa, D. E. Huber, B. Welk, H. L. Fraser, Development and application of 32 MIPARTM: A novel software package for two- and three-dimensional microstructural characterization. *Integr. Mater. Manuf. Innov.* **3**, 10 (2014).
43. R Core Team, *R: A Language and Environment for Statistical Computing* (R Foundation for Statistical Computing, Vienna, Austria, 2019).
44. H. Wickham, *ggplot2: Elegant Graphics for Data Analysis* (Springer, New York, 2016).
45. H. Li, R. Durbin, Fast and accurate short read alignment with Burrows-Wheeler transform. *Bioinformatics* **25**, 1754–1760 (2009).
46. I. Milne *et al.*, Using Tablet for visual exploration of second-generation sequencing data. *Brief. Bioinform.* **14**, 193–202 (2013).